chemosensors

MDPI

Article

Polymer Nanoparticle Identification and Concentration Measurement Using Fiber-Enhanced Raman Spectroscopy

Mark R. Pollard [1,†], Katia Sparnacci [2], Lars J. Wacker [1] and Hugo Kerdoncuff [1,*]

[1] Danish Fundamental Metrology, Kogle Allé 5, 2970 Hørsholm, Denmark; Mark.Pollard@3shape.com (M.R.P.); ljw@dfm.dk (L.J.W.)

[2] Dipartimento di Scienze e Innovazione Tecnologica, Università degli Studi del Piemonte Orientale "A. Avogadro", viale T. Michel 11, 15121 Alessandria, Italy; katia.sparnacci@uniupo.it

* Correspondence: hk@dfm.dk

† Current address: 3Shape A/S, Holmens Kanal 7, 1060 Copenhagen, Denmark.

Received: 30 January 2020; Accepted: 11 March 2020; Published: 14 March 2020

Abstract: We present a measurement technique for chemical identification and concentration measurement of polymer nanoparticles in aqueous solution, which is achieved using Raman spectroscopy. This work delivers an improvement in measurement sensitivity of 40 times over conventional Raman measurements in cuvettes by loading polymer nanoparticles into the hollow core of a microstructured optical fiber. We apply this "fiber-enhanced" system to measure the concentration of two separate samples of polystyrene particles (diameters of 60 nm and 120 nm respectively) with concentrations in the range from 0.07 to 0.5 mg/mL. The nanoliter volume formed by the fiber presents unique experimental conditions where nanoparticles are confined within the fiber core and prevented from diffusing outside the incident electromagnetic field, thereby enhancing their interaction. Our results suggest an upper limit on the size of particle that can be measured using the hollow-core photonic crystal fiber, as the increasing angular distribution of scattered light with particle size exceeds the acceptance angle of the liquid-filled fiber. We investigate parameters such as the fiber filling rate and optical properties of the filled fiber, with the aim to deliver repeatable and quantifiable measurements. This study thereby aids the on-going process to create compact systems that can be integrated into nanoparticle production settings for in-line measurements.

Keywords: nanoparticle measurement; concentration; optical fiber; Raman spectroscopy

1. Introduction

The application of nanoparticle technologies has revolutionised the development of new materials with enhanced physical characteristics (including mechanical, chemical and electromagnetic) [1,2] and resulted in new products in a diverse range of areas, such as lighting [3], flexible electronics [4], catalytic processes [5], pharmaceuticals [6] and biomedical research [7]. The optimization of material properties is reliant on the precise control of nanoparticle concentration and the subsequent need for sensitive, reliable and fast concentration measurement within typical environments (e.g., nanoparticle in aqueous solution) [8,9].

Established concentration measurement techniques [9] such as Resistive Pulse Sensing (RPS) or Quartz Crystal Microgravimetry (QCM), provide meaningful data where nanoparticle characteristics are known a-priori (for example, conductivity in RPS measurements or density and size in QCM measurements) and have been produced without contamination. Transmission electron microscopy [10] provides images of nanoparticle size and distribution but requires particle fixation on a surface and cannot distinguish between desired nanoparticles and unwanted contamination with similar dimensions. In contrast, Inductively-Coupled Plasma Mass Spectroscopy (ICPMS) [11]

can identify precisely the type and quantity of materials present but requires samples to be ionized/decomposed in plasma, which can be far removed from the intended usage conditions.

Optical techniques provide a non-destructive measurement of nanoparticles in aqueous solution with minimal requirements for sample preparation. Experimental observations of optical scattering by nanoparticles within localized evanescent optical fields have enabled individual nanoparticles to be detected [12,13] and metallic particles are measured often using the surface plasmon resonance that is generated from their irradiation with broadband light [14]. Light scattering techniques provide flexible and relatively simple measurements of particle diameter based on ensembles of nanoparticles [15] and more recent techniques employ sophisticated computer algorithms to track and identify nanoparticles [10]. These techniques are ultimately limited by the scattering coefficient of the nanoparticles (which is highest for metallic particles) and the optical system, specifically limitations in focal volume, resolution and unwanted absorption or emission of light.

In this study, we improve the optical system by applying unique optical fiber technology, namely hollow-core photonic crystal fiber (HC-PCF), to enhance spectroscopic measurements on nanoparticles. The HC-PCF (referred to as the 'fiber') is made from silica and consists of a hollow honeycomb structure and a central core with a typical diameter of tens of micrometers [16]. The optical enhancement arises from the confinement of both the incident laser light and the sample under test within a volume that extends along the length of the fiber. Consequently, problems relating to diffusion of particles outside of the light beam are minimized. A fiber with a length of several centimeters can be filled easily with liquid using capillary forces [17] and the unique nanoliter volume formed by the fiber has enabled new experiments to be performed on small populations (10^6 particles) of nanoparticles [18].

We have investigated the use of fiber-enhanced Raman spectroscopy (FERS), a laser-based optical spectroscopy technique [19], to provide chemical-specific identification of nanoparticles and measurement of nanoparticle concentration in aqueous solution. Raman spectroscopy is a well-known technique for chemical-specific, non-destructive characterization of a wide variety of samples [20], including nanomaterials [21–23]. It generally requires little to no sample preparation, which makes it applicable for in-line measurements in production settings. However, Raman scattering is a weak process that usually requires measurement times of several minutes to detect concentrations below 1 mg/mL. We overcome the problem of the very low intensity of Raman scattering signals from nanoparticles by loading them into the hollow core of the fiber and using the tight confinement of the light in the guided mode of the fiber to probe them efficiently. Different hollow capillaries have been investigated for this purpose in earlier studies (e.g., Teflon capillaries and HC-PCF) [24]. Compared to other enhanced Raman techniques, such as surface-enhanced Raman spectroscopy (SERS) [25,26] and tip-enhanced Raman spectroscopy (TERS) [27], FERS is usually less sensitive but is non-destructive and necessitates only very small volumes of samples on the order of a few nanoliters. Moreover, the signal enhancement does not come from a change in Raman scattering cross sections but from an increased light-matter interaction due to the optical confinement in the fiber core, which preserves the relative peak intensities of Raman spectra. Hence, Raman spectra obtained by FERS can be readily compared to the databases of Raman spectra measured by conventional spontaneous Raman spectroscopy.

FERS has been applied previously with nanomaterials for the characterization of zinc oxide nanoparticles [28] and cadmium telluride quantum dots [29]. It has also attracted interest in biosensing and pharmaceutical sciences, where it has seen major technological development and achieved state-of-the-art sensitivity in recent years [30,31].

We have demonstrated quantitative FERS measurements on polystyrene nanoparticles in water by normalizing Raman signals against a reference signal that takes into account the variation in optical transmission of light through the fiber. Since polystyrene does not present significant absorption [32] of the incident laser light or of the Raman scattered light in the region of interest (optical wavelengths from 530 nm to 590 nm), we expect that the optical properties of a fiber-loaded with polystyrene

nanoparticles are solely determined by refractive index difference within the fiber (between the liquid core and the silica surrounding) and the scattering of light by nanoparticles.

2. Materials and Methods

2.1. Nanoparticle Preparation

Two batches of polystyrene nanoparticles with diameters about 120 nm and 60 nm, marked PS120 and PS60 respectively, were prepared separately. The polystyrene nanoparticles were prepared from styrene (Sigma-Aldrich) which was purified by passing through an inhibitor removal column (Sigma-Aldrich). Sodium dodecyl sulfate (SDS) and potassium persulfate (KPS) were purchased from Sigma-Aldrich and used without further purification. The polystyrene nanoparticles were synthesized by emulsion polymerization. The polymerization reactions were carried out in a 1 L five-neck reactor equipped with a condenser, a mechanical stirrer, a thermometer and inlets for nitrogen and styrene. 500 mL of deionized water containing the appropriate amount of SDS (0.3 g, corresponding to 1.0 mmol, for PS120 particles and 1.0 g, corresponding to 3.5 mmol for PS60 particles) were introduced into the reactor at room temperature with a stirring rate of 300 rpm, then 30.0 mL (0.26 mol) of styrene were added dropwise. The mixture was purged with nitrogen, and nitrogen was fluxed during the entire polymerization procedure. The reactor was heated to 80 °C, then a potassium persulfate aqueous solution (5.0 mL, 0.74 mmol) was added, and the mixture was reacted for 24 h. The obtained latex was purified from surfactant and unreacted monomer by repeated dialyses against ultrapure water (cellulose membrane, molecular weight cut-off 12 kDa). Particle size and size distribution were measured by scanning electron microscopy (SEM), as shown on Figure 1. The microscope was an Inspect F SEM-FEG (Field Emission Gun) from FEI company, with a beam diameter of 3 nm, equipped with EDAX microanalysis. The SEM micrographs were analyzed by the ImageJ image processing program. Approximately 300 individual nanoparticle diameters were measured for each sample. The measured values for the two samples using this instrument were found to be 121 nm $\pm$ 5 nm for sample PS120 and 63 nm $\pm$ 5 nm for sample PS60. Dynamic light-scattering analysis was performed at 25 °C with a Malvern Zetasizer Nano ZS equipped with a 4 mW He-Ne laser. Each value is the average of five measurements. The instrument was calibrated against standard polystyrene latex with a diameter of 200 nm. The resulting measurements on the particle hydrodynamic radii were found to be 139 (PDI 0.015) for sample PS120 and 65 nm (PDI 0.025) for sample PS60. The particle concentration was determined gravimetrically. In details, five aliquots of 1.00 mL of nanoparticle suspension were placed in pre-weighed aluminum dishes and dried in a vacuum oven at 80 °C for 24 h, then weighed to quantify the residual, the reported result was the medium of the five measurements and the relative standard deviation is ≈3%. The particle number concentration was derived from the mass concentration and the particle diameter, assuming a particle density of 1.04 g/mL. A concentration series of nanoparticle samples were made by diluting the stock nanoparticle solution in MilliQ water.

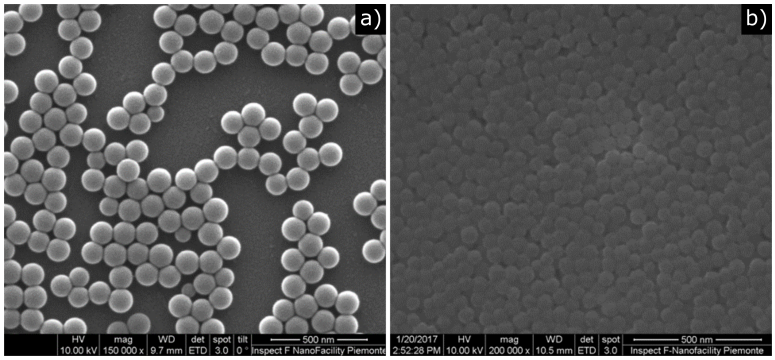

Figure 1. Representative scanning electron microscopy (SEM) image of the polystyrene nanoparticles: (**a**) sample PS120, (**b**) sample PS60.

2.2. Fiber Preparation and Filling

The fiber is made from HC-PCF (HC1060 from NKT Photonics, Birkerød, Denmark) that was cut in lengths of 10 cm ± 1 cm. Fiber coating was removed from the ends of the fiber and then both ends of the fiber were collapsed using a fusion splicer [33], which allowed the nanoparticle sample to be loaded precisely into the 10 µm diameter fiber core. The fiber ends were fixed using nail polish into separate glass enclosures. These enclosures acted as a container for the nanoparticle sample while allowing light to be coupled in and out of the fiber.

Initial experiments were made to confirm that the central hollow core was filled correctly, by loading a blue ink solution into a prepared fiber and timing the arrival of blue ink at the far end of the fiber (see Figure 2). Capillary forces drive this filling process and the measured filling time (180 s) agrees with previous work on fiber loading [17]. To avoid unwanted evaporation of liquid within the fiber over several hours, it was necessary to enclose both ends of the prepared fiber.

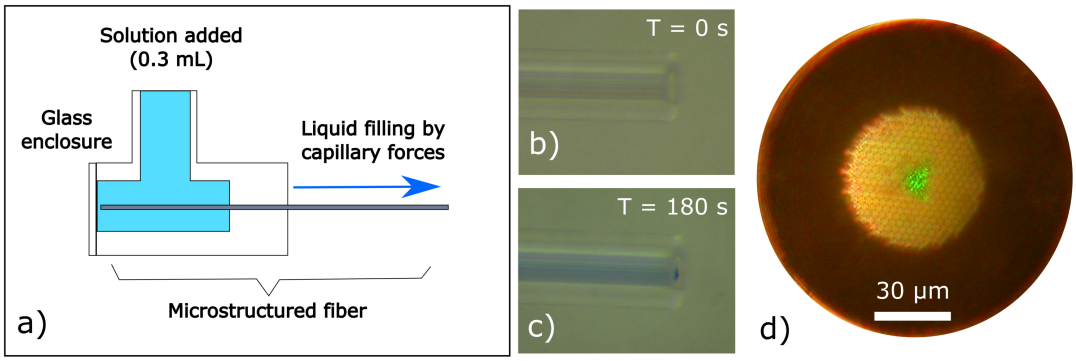

Figure 2. Fiber filling experiments: (**a**) schematic of sample loading into a prepared fiber that is encased in a glass enclosure. (**b**,**c**) Microscope images showing the loading of blue ink into the fiber, at the start (**b**) and at the end (**c**) of the process. (**d**) Microscope image showing the transmission of green laser light in the filled fiber core. The image is taken from a cleaved end of the fiber after sample loading. The fiber outer diameter is 125 µm with a fiber core diameter of 10 µm and a diameter of 50 µm for the holey region.

Figure 3 shows a schematic of the optical setup that was created to measure nanoparticle concentrations in aqueous samples loaded into the core of a fiber.

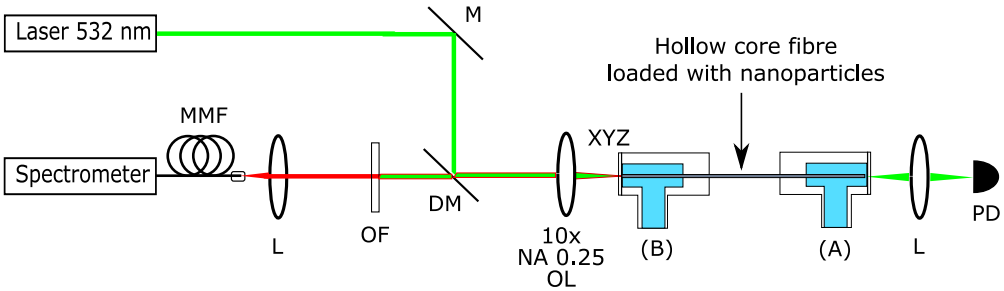

Figure 3. Optical setup for measurement of nanoparticle solution loaded into HC-PCF. Nanoparticle samples were loaded in enclosure (A) and filled the fiber by capillary action towards enclosure (B). Laser light travelled through the fiber from (B) to (A), with back-scattered Raman light travelling in the opposite direction. L: lens; OF: optical filter; M: mirror; DM: dichroic mirror; OL: objective lens; XYZ: translation stage; PD: photodetector; MMF: multimode optical fiber.

Loading of the nanoparticle solution was achieved using a syringe and needle (VWR luer-lock syringe 2 mL and Sterican needle) to load the solution at one end of the prepared fiber, marked as (A) in Figure 3.

Laser light was sent into the fiber from a Coherent Verdi laser operating at 532 nm wavelength. A dichroic mirror (Semrock LPD02-532RU-25) reflected the excitation light into an objective lens (Olympus 10×, 0.3 NA) that focussed the light on the fiber. Precise micrometer alignment of the fiber relative to the focused laser beam was achieved by mounting the input end of the fiber (marked as (B) in Figure 3) onto a 3-axis translation stage (Thorlabs MBT616D), then maximizing the optical power transmitted through the fiber using a photodetector.

The input laser light generated Raman scattering from the nanoparticle sample contained in the fiber. A fraction of the Raman scattered light was back-scattered (i.e., opposite to the direction of laser propagation) which is a well-known configuration for Raman spectroscopy [34]. The Raman scattered light was collected and analyzed after passing through a long-pass optical filter (Semrock RazorEdge 532RU Long Pass) to remove any residual excitation laser light and then sent by a standard solid-core step-index optical fiber to a Raman spectrometer (Horiba iHR320).

Light guiding in the core of the liquid-filled fiber after alignment to the laser beam was confirmed by observing laser light emerging from the fiber tip at the end of the length of fiber (see Figure 2d). The numerical aperture of the selectively filled fiber was calculated based on previous work by Eftekhari et al. [35] that reported an effective cladding refractive index of 1.17. The numerical aperture (NA) of a step-index fiber is given by

$$NA = n_{surrounding} \sin \theta_c = \sqrt{n_{core}^2 - n_{clad}^2}, \quad (1)$$

with n being the refractive index of the core, cladding and surrounding material of the fiber respectively, and θ_c the maximum acceptance angle of the fiber. Figure 4 shows a cross-section of the filled fiber and the different refractive indices.

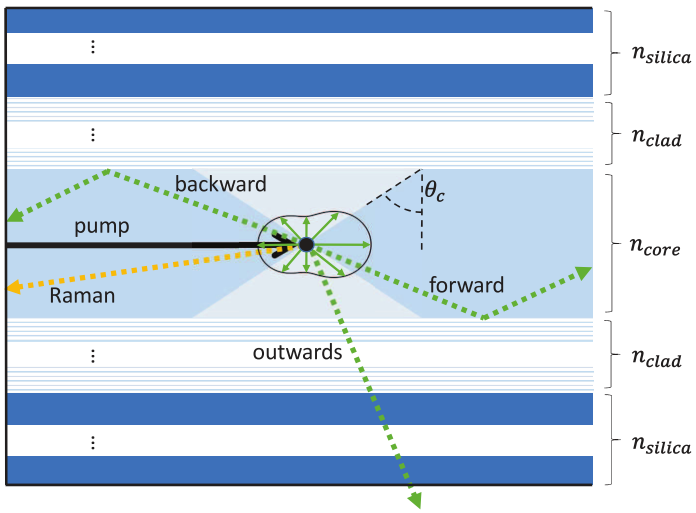

Figure 4. Schematic drawing of the scattering process on a nanoparticle inside a fiber. Laser light (pump) is coupled into the fiber from the left side and scattered on a nanoparticle. For illustrative purposes, a spatial distribution of the scattering angles for Mie-scattering on nanoparticles is shown. Light scattered under an angle larger than the critical angle θ_c with respect to the cladding is guided inside the core (forward and backward). For angles smaller than the critical angle, the light is not guided within the fiber core and scattered outwards. Only Raman-scattered light in the backward direction contributes to the signal. For illustrative purposes, only a single nanoparticle is shown. The correct proportions of the cladding and holey region are shown in Figure 2.

The NA value (0.63) was used to calculate the V number [36] associated with the fiber, which is an indication of optical field created within the fiber and is given by

$$V = \frac{2\pi a}{\lambda} NA, \tag{2}$$

where a is the core diameter and λ is the laser wavelength. For a core diameter of 10 µm, a V number of 74 was calculated at 532 nm wavelength, indicating that the fiber behaved as a lossy multi-mode waveguide.

3. Results and Discussion

The Raman spectrum from a HC-PCF filled with a sample of polystyrene nanoparticles diluted in water is shown in Figure 5a. The spectrum contains three components; a small set of peaks in the region below 800 cm^{-1} created by Raman scattering of light by the silica molecules in the fiber [37], a small peak arising from the O-H vibrational bending mode of water molecules is observed at 1640 cm^{-1} and a very large peak arising from several O-H vibrational stretching modes of water molecules around 3200 cm^{-1} in agreement with literature reports [38]. Measurement of sample PS60 in solution with a longer acquisition time in the region 900–1600 cm^{-1} is shown in Figure 5b. Here we can see more clearly the peaks arising from polystyrene at 1001 cm^{-1}, created by a vibrational mode arising from the substituted benzene ring present in polystyrene [39], and from the O–H bending mode of the water molecules at 1640 cm^{-1}.

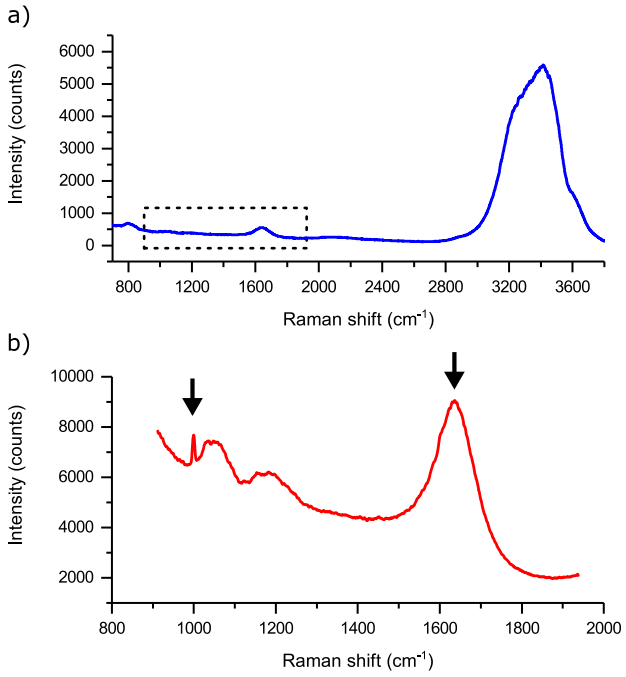

Figure 5. Fiber-enhanced Raman spectra of polystyrene nanoparticles in aqueous solution. (**a**) Full-spectrum showing Raman scattering originating from water and silica in the fiber, dominated by scattering from the O–H stretching mode of water molecules. The spectrum is the average of two acquisitions, with an integration time of five seconds each, and a laser excitation power of 1.7 mW. A second measurement was made as shown in (**b**) with arrows denoting the peaks arising from polystyrene and water. The spectrum has limits as shown by the dotted box in Figure 5a and is the average of ten acquisitions, with an integration time of ten seconds each, and a laser excitation power of 50 mW. The peaks around 1050 cm^{-1} and 1200 cm^{-1} are caused by the silica walls of the hollow-core photonic crystal fiber (HC-PCF).

The large peak created by the O-H stretching mode provides direct evidence for the enhancement created by the HC-PCF and would be significantly smaller if the fiber was not aligned correctly to the incident laser light. We calculate that the Raman scattering signals are enhanced by a factor of 40 times by this optical system, by comparing the peak height of the O–H stretching mode for cases where the fiber is aligned correctly and where the laser is simply incident on the bulk solution contained in the glass enclosure, as shown in Figure 6.

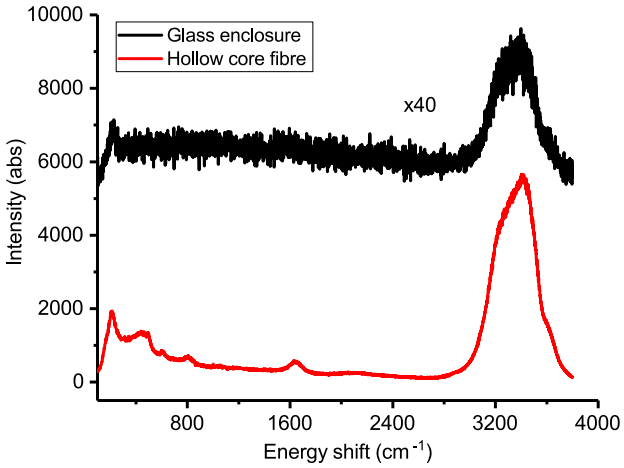

Figure 6. Raman spectra of polystyrene nanoparticles in aqueous solution measured in the bulk solution in the glass enclosure (black) and in the HC-PCF (red). Both measurements were made with the same measurement parameters (e.g., optical power, acquisition time). To enable comparison between the two spectra, the bulk solution spectra has been multiplied by a factor of 40 as shown.

The ratio of the heights of the peak at 1001 cm^{-1} to the peak at 1640 cm^{-1} allows the amount of polystyrene nanoparticles to be quantified as demonstrated in Figure 7a. This shows measurements for a dilution series of PS60 nanoparticles, for concentrations in the range 3.3×10^{11} particles/mL up to 4.9×10^{12} particles/mL, based on a stock concentration of 3.29×10^{14} particles/mL. Measurements were repeated three times per concentration with a new fiber and nanoparticle sample used for each measurement. We observed that the spectra remained constant over several hours.

The minimum values of the two Raman peaks were affected by the presence of small Raman signals created by vibrational modes in silica molecules within the fiber walls [37] (see Figure 5b). We compensated for the presence of the unwanted signals by calculating the base of the Raman peak from the average of two values at either side of the peak.

The data in Figure 7a shows that the Raman peak height ratio increases with the concentration of polystyrene nanoparticles. The upper limit for concentration measurement was found to be 3.70×10^{12} particles/mL. Above this value, the amount of transmitted light through the fiber was low (≈6%, see Figure 7b and no Raman signals from the nanoparticles were observed. A linear fit to a subset of the Raman peak ratio data was calculated using the least-squares method in DFM LSQ software [40] with a R^2 coefficient of 0.97. The limit of detection for the measurement of polystyrene nanoparticles was calculated to be 0.92×10^{12} particles/mL, based on the ratio of Raman peaks (R_{LWR}) measured for three control samples with no nanoparticles present (MilliQ water sample loaded into the fiber). This lower limit was calculated from

$$R_{LWR} = \bar{x} + 3\sigma_{CTRL}, \quad (3)$$

where $\bar{x}$ is the mean Raman peak ratio and σ_{CTRL} is the standard deviation for the control measurements. The limit of detection was then found from the corresponding concentration value in the linear fit as shown in Figure 7a.

The reduction in the laser power transmitted through the fiber for increasing concentrations of nanoparticles (see Figure 7b), suggests that insufficient light was being guided in the core of the fiber and instead light was guided in the fiber cladding. This conclusion is supported by the significant increase in the silica signal observed as the fiber cladding interacts with the laser light (see Figure 7c). This shows that the maximum concentration of nanoparticles that can be measured using this system is limited by the ability of the fiber to guide light while its core is filled with nanoparticles. This upper limit is determined by the angular distribution of light scattered by the particles and the corresponding range of angles that can be guided by the HC-PCF (the NA value calculated in Equation (1)).

As increasing concentration breaks the guiding in the fiber, the particle size also increases. A series of three measurements at a concentration of 1.7×10^{11} particles/mL of sample PS120 (particle diameter of 121 nm $\pm$ 5 nm measured by SEM) confirmed the increased scattering of light out of the fiber core and into the silica cladding. The resulting reduced transmission of the excitation laser light inhibited the enhancement of Raman scattering from the nanoparticle solution, while the larger silica contribution to the Raman spectra prevented the observation of the Raman peaks of polystyrene. Measurements at lower concentrations of sample PS120, i.e., 5.0×10^{9} particles/mL and 2.0×10^{10} particles/mL, showed less Raman scattering from silica but were below the limit of sensitivity of the system. We conclude that the unfavorable balance between sensitivity and light guiding of the fiber with polystyrene particles of diameters of at least 120 nm limits the application of the measurement method to smaller nanoparticle sizes.

We confirmed our observations by simulating the expected scattering distribution from the two sizes of nanoparticles. We calculated the angle-dependent Mie scattering distribution for the two different particle sizes using the MATLAB functions for Mie scattering by C. Mätzler [41]. In accordance with the principles presented for Equation (1), we numerically calculate the scattering amplitude inside the fiber. We differentiate three cases for light scattered by a nanoparticle as illustrated in Figure 4. Light scattered with an angle smaller than the acceptance angle $\alpha < \theta_c$ given by Equation (1) is considered unaffected and continues guided within the fiber. Light scattered backwards $\alpha > \pi - \theta_c$ partially Raman scatters with a certain probability (typically 1 in 10 million scattering events). Light scattered backwards without changing wavelength is taken into account when calculating the total pump light intensity. However, within the length of fiber considered in our experiments, the contributions from backwards scattered light to the pump light can be neglected. Light scattered under an angle larger than the critical angle ($\pi - \theta_c > \alpha > \theta_c$) cannot be guided by the fiber core and is treated as lost. We note that the transition between silica and air on the outer side of the fiber is providing a larger acceptance angle than the fiber core due to the larger difference in the index of refraction. Light scattered out of the fiber core is thus partially confined to the inside of the silica of the fiber. However, since the confining volume is considerably larger than the core region, the intensity within the core is very small, thus the contribution can be neglected. The amount of light transmitted through the fiber can be described by the Beer–Lambert-law

$$P(d) = P_0 e^{-\epsilon d}, \tag{4}$$

with P_0 being the power coupled into the fiber, ϵ being the scattering coefficient, d the distance transmitted through the fiber. Our simulations directly supply absolute values for the loss coefficient due to scattering at the nanoparticles and has been used to simulate the loss through the fiber. The results have been adjusted by means of P_0 to fit the measured values with no nanoparticles present and the results are shown together with the experimental results in Figure 7b.

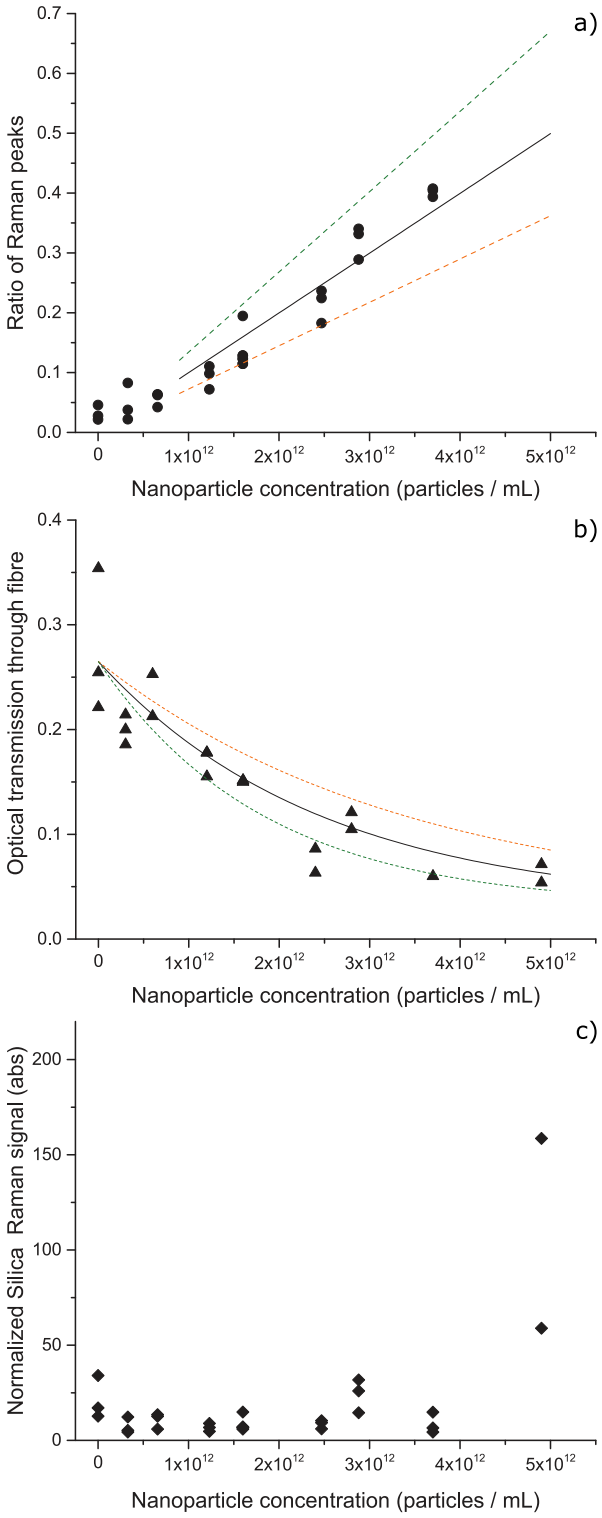

Figure 7. Experimental measurements on PS60 nanoparticles in aqueous solution. (**a**) Variation of Raman peak ratio with nanoparticle concentration. Measurements (circles), simulation for 63 nm (solid line), 58 nm (orange dashed line) and 68 nm (green dashed line). (**b**) Variation of optical power transmitted through the optical fiber (measurements shown as triangles) with simulation results for particles with diameter of 63 nm (solid line), 58 nm (orange dashed line) and 68 nm (green dashed line). (**c**) Variation of the peak height of silica at 490 cm^{-1} normalized to the peak height of the O–H stretching mode, for increasing concentrations of nanoparticles.

The position-dependent attenuation of the exciting laser light on the Raman scattering process is taken into account. The total signal of the Raman scattering signal from the nanoparticles is obtained by summing all scattering amplitudes over the length of the fiber for the nanoparticles, as well as for the water.

We found that the larger nanoparticle scatters a significantly larger proportion of the laser light which leads to a break-down in the light-guiding properties of the fiber and the undesired propagation of light out of the confines of the fiber's central core and the subsequent generation of large Raman scattering signals by the silica in the fiber walls.

Evidence for the loading of nanoparticles along the length of the fiber was observed when the fiber was cut (a process known as cleaving) at a position after the glass enclosure (marked as (B) in Figure 3). After the optical realignment of the fiber, Raman spectra showed an increase in the polystyrene signal from the cut end of the fiber. This increase in signal occurred over several hours and we consider this effect to be caused by an agglomeration of nanoparticles as the water evaporates from the cut end of the fiber. We emphasize that the bulk nanoparticle solution was loaded at the enclosed end of the fiber (marked as (A) in Figure 3) and not the cut end of the fiber. In addition, the Raman signals remained constant before cutting the fiber, which suggests the signal increase is caused solely by exposing one end of the fiber that contains the nanoparticle solution.

4. Conclusions

We have demonstrated a measurement method for polymer nanoparticle characterization by providing chemical-specific identification and concentration measurements of polystyrene nanoparticles. Our use of fiber-enhanced Raman spectroscopy allows nanoparticle characterization in a non-destructive manner on samples that are in aqueous solution. This technique has significant potential to provide important information on nanoparticles, with application for novel drug-delivery methods involving polymer nanoparticles [2,23], for example.

We have investigated the process of filling the nanoparticle solution into the fiber and found that nanoparticles can be loaded in a repeatable fashion and are present along the length of the fiber. Enclosure of both ends of the fiber is required to prevent agglomeration of particles and changes in concentrations due to the evaporation of water. One significant advantage of fiber-based measurement is the requirement of very small nanoliter volumes of samples only, which is advantageous for analyzing expensive materials or samples with limited available quantities. Future improvement of our measurement system may include microfluidics technology for reducing the amount of sample required for sample handling. Important work is also required to determine the chemical interaction between the nanoparticles and the internal walls of the silica optical fiber, and its influence on FERS measurements. We note that established techniques such as capillary electrophoresis have addressed the problem of undesired particle interaction with silica surfaces and we envisage this knowledge can be applied in future fiber-enhanced studies.

Our work confirms that HC-PCF technology provides a mechanism for significantly enhancing optical signals by increasing the interaction between light and sample. Further study of the optical signals generated by the nanoparticles could reveal information on particle shape and size. The fiber-enhancement technique can increase Raman scattering signals by one to two orders of magnitude. The enhancement remains lower in comparison to SERS but the technique does not require contamination of the sample with metal particles of chemical attachment to a surface and can be simply achieved by diluting the sample in solution and loading it into the fiber. Our results demonstrate an enhancement of the Raman signal by 40 compared to bulk measurements in cuvettes.

We have shown that the size of nanoparticle that can be measured with our FERS system is limited by the optical guiding capabilities of the fiber while loaded with the nanoparticle solution. Mie scattering of light by relatively large particles inhibits the fiber-enhancement mechanism and leads to increased background signal by scattering light into the silica cladding. Between the two types of nanoparticle that we investigated, we could not detect a Raman signal from the larger ones,

with diameters of 121 nm ± 5 nm, due to the limited sensitivity at low concentrations and poor guiding at higher concentrations. Concentrations of the smaller nanoparticles with diameters of 63 nm ± 5 nm were measured within the range 0.92×10^{12} particles/mL to 3.72×10^{12} particles/mL. The higher concentration limit was also due to poor guiding in the fiber core resulting from the higher number of scatterers. Improvement to the guiding of optical signals within the fiber core and reduction of unwanted background signal can be achieved using alternative designs of the optical fiber with higher NA and lower amount of silica surrounding the guiding core [31,42], refining the fiber preparation method (and the related collapse of the photonic crystal structure [30]), and optimizing the length of the optical fiber according to the transmission properties of the solution. Further improvements to the sensitivity of nanoparticle concentration measurement can be achieved by combining our fiber-enhanced system with Raman enhancement techniques that target specific vibrational modes, such as resonance Raman scattering [43] or stimulated Raman scattering [44].

Author Contributions: conceptualization, M.R.P. and H.K.; methodology, M.R.P., L.J.W., K.S. and H.K.; validation, M.R.P. and H.K.; formal analysis, M.R.P., L.J.W. and H.K.; investigation, M.R.P. and H.K.; resources, K.S.; data curation, M.R.P.; writing—original draft preparation, M.R.P.; writing—review and editing, H.K.; visualization, M.R.P., L.J.W., K.S. and H.K.; supervision, M.R.P.; project administration, M.R.P.; funding acquisition, M.R.P. All authors have read and agreed to the published version of the manuscript.

Funding: This research was funded by the European Metrology Programme for Innovation and Research (EMPIR) as part of the InNanoPart 14IND12 project. The EMPIR initiative is co-funded by the European Union's Horizon 2020 research and innovation programme and by the EMPIR participating states. This research was co-funded by the Danish Agency for Institutions and Educational Grants.

Acknowledgments: We thank DFM colleagues (Lars Nielsen, Mikael Lassen and Jan C. Petersen) for useful discussions and comments on the manuscript.

Conflicts of Interest: The authors declare no conflict of interest. The funders had no role in the design of the study; in the collection, analyses, or interpretation of data; in the writing of the manuscript, or in the decision to publish the results.

References

1. Lue, J.-T. A review of characterization and physical property studies of metallic nanoparticles. *J. Phys. Chem. Solids* **2001**, *62*, 1599–1612. [CrossRef]
2. Nasir, A.; Kausar, A.; Younus, A. A Review on Preparation, Properties and Applications of Polymeric Nanoparticle-Based Materials. *Polym. Plast. Technol. Eng.* **2015**, *54*, 325–341. [CrossRef]
3. Shirasaki, Y.; Supran, G.J.; Bawendi, M.G.; Bulovic, V. Emergence of colloidal quantum-dot light-emitting technologies. *Nat. Photonics* **2013**, *7*, 13–23. [CrossRef]
4. Shen, W.; Zhang, X.; Huang, Q.; Xu, Q.; Song, W. Preparation of solid silver nanoparticles for inkjet printed flexible electronics with high conductivity. *Nanoscale* **2014**, *6*, 1622–1628. [CrossRef] [PubMed]
5. Schauermann, S.; Nilius, N.; Shaikhutdinov, S.; Freund, H.-J. Nanoparticles for Heterogeneous Catalysis: New Mechanistic Insights. *Acc. Chem. Res.* **2013**, *46*, 1673–1681. [CrossRef] [PubMed]
6. Sheth, P.; Sandhu, H.; Singhal, D.; Malick, W.; Shah, N.; Kislalioglu, M.S. Nanoparticles in the pharmaceutical industry and the use of supercritical fluid technologies for nanoparticle production. *Curr. Drug Deliv.* **2012**, *9*, 269–284. [CrossRef]
7. Byrne, J.D.; Betancourt, T.; Brannon-Peppas, L. Active targeting schemes for nanoparticle systems in cancer therapeutics. *Adv. Drug Deliv. Rev.* **2008**, *60*, 1615–1626. [CrossRef]
8. Lisinger, T.P.J.; Roebben, G.; Gilliland, D.; Calzolai, L.; Rossi, F.; Gibson, N.; Klein, C. *Requirements on Measurements for the Implementation of the European Commission Definition of the Term 'Nanomaterial'*; Publications Office of the European Union: Brussels, Belgium, 2012; p. JRC73260.
9. Brown, S.C.; Boyko, V.; Meyers, G.; Voetz, M.; Wohlleben, W. Toward advancing nano-object count metrology: A best practice framework. *Environ. Health Perspect.* **2013**, *121*, 1282–1291. [CrossRef]
10. Domingos, R.F.; Baalousha, M.A.; Ju-Nam, Y.; Reid, M.M.; Tufenkji, N.; Lead, J.R.; Leppard, G.G.; Wilkinson, K.J. Characterizing Manufactured Nanoparticles in the Environment: Multimethod Determination of Particle Sizes. *Environ. Sci. Technol.* **2009**, *43*, 7277–7284. [CrossRef]

11. Proulx, K.; Wilkinson, K.J. Separation, detection and characterisation of engineered nanoparticles in natural waters using hydrodynamic chromatography and multi-method detection (light scattering, analytical ultracentrifugation and single particle ICP-MS). *Environ. Chem.* **2014**, *11*, 392–401. [CrossRef]
12. Yang, S.; Taflove, A.; Backman, V. Experimental confirmation at visible light wavelengths of the backscattering enhancement phenomenon of the photonic nanojet. *Opt. Express* **2011**, *19*, 7084–7093. [CrossRef] [PubMed]
13. Wheaton, S.; Gelfand, R.M.; Gordon, R. Probing the Raman-active acoustic vibrations of nanoparticles with extraordinary spectral resolution. *Nat. Photonics* **2015**, *9*, 68–72. [CrossRef]
14. Haiss, W.; Thanh, N.T.K.; Aveyard, J.; Ferning, D.G. Determination of Size and Concentration of Gold Nanoparticles from UV-Vis Spectra. *Anal. Chem.* **2007**, *79*, 4215–4221. [CrossRef] [PubMed]
15. Brar, S.K.; Verma, M. Measurement of nanoparticles by light-scattering techniques. *TrAC Trends Anal. Chem.* **2011**, *30*, 4–17. [CrossRef]
16. Russel, P. Photonic Crystal Fibers. *Science* **2003**, *299*, 358–362. [CrossRef]
17. Nielsen, K.; Noordegraaf, D.; Sørensen, T.; Bjarklev, A.; Hansen, T.P. Selective filling of photonic crystal fibres. *J. Opt. A Pure Appl. Opt.* **2005**, *7*, L13–L20. [CrossRef]
18. Zuber, A.; Purdey, M.; Schartner, E.; Forbes, C.; van der Hoek, S.; Giles, D.; Abell, A.; Monro, T.; Ebendorff-Heidepriem, H. Detection of gold nanoparticles with different sizes using absorption and fluorescence based method. *Sens. Actuator B-Chem.* **2016**, *227*, 117–127. [CrossRef]
19. Colthup, N.B.; Daly, L.H.; Wiberly, S.E. *Introduction to Infrared and Raman Spectroscopy*; Academic Press: New York, NY, USA, 1990.
20. Das, R.S.; Agrawal, Y.K. Raman spectroscopy: Recent advancements, techniques and applications. *Vib. Spectrosc.* **2011**, *57*, 163–176. [CrossRef]
21. Kumar, C.S.S.R. *Raman Spectroscopy for Nanomaterials Characterization*; Springer: Berlin/Heidelberg, Germany, 2012.
22. Ye, K.; Li, K.; Lu, Y.; Guo, Z.; Ni, N.; Liu, H.; Huang, Y.; Ji, H.; Wang, P. An overview of advanced methods for the characterization of oxygen vacancies in materials. *Trends Anal. Chem.* **2019**, *116*, 102–108. [CrossRef]
23. Vanden-Hehir, S.; Tipping, W.J.; Lee, M.; Brunton, V.G.; Williams, A.; Hulme, A.N. Raman Imaging of Nanocarriers for Drug Delivery. *Nanomaterials* **2019**, *9*, 341. [CrossRef] [PubMed]
24. Mak, J.S.W.; Rutledge, S.A.; Abu-Ghazalah, R.M.; Eftekhari, F.; Irizar, J.; Tam, N.C.M.; Zheng, G.; Helmy, A.S. Recent developments in optofluidic-assisted Raman spectroscopy. *Prog. Quantum Electron.* **2013**, *37*, 1–50. [CrossRef]
25. Schmidt, M.S.; Hübner, J.; Boisen, A. Large Area Fabrication of Leaning Silicon Nanopillars for Surface Enhanced Raman Spectroscopy. *Adv. Mater.* **2012**, *24*, OP11–OP18. [CrossRef] [PubMed]
26. Lim, D.-K.; Jeon, K.-S.; Kim, Y.M.; Nam, J.-M.; Suh, Y.D. Nanogap-engineerable Raman-active nanodumbbells for single-molecule detection. *Nat. Mater.* **2010**, *9*, 60–67. [CrossRef] [PubMed]
27. Verma, P. Tip-Enhanced Raman Spectroscopy: Technique and Recent Advances. *Chem. Rev.* **2017**, *117*, 6447–6466. [CrossRef]
28. Irizar, J.; Dinglasan, J.; Goh, J.B.; Khetani, A.; Anis, H.; Anderson, D.; Goh, C.; Helmy, A.S. Raman Spectroscopy of Nanoparticles Using Hollow-Core Photonic Crystal Fibers. *IEEE J. Sel. Top. Quantum Electron.* **2008**, *14*, 1214–1222. [CrossRef]
29. Mak, J.S.W.; Farah, A.A.; Chen, F.; Helmy, A.S. Photonic crystal fiber for efficient Raman scattering of CdTe quantum dots in aqueous solution. *ACS Nano* **2011**, *5*, 3823–3830. [CrossRef]
30. Yan, D.; Popp, J.; Pletz, M.W.; Frosch, T. Highly Sensitive Broadband Raman Sensing of Antibiotics in Step-Index Hollow-Core Photonic Crystal Fibers. *ACS Photonics* **2017**, *4*, 138–145. [CrossRef]
31. Yan, D.; Frosch, T.; Kobelke, J.; Bierlich, J.; Popp, J.; Plets, M.W.; Frosch, T. Fiber-Enhanced Raman Sensing of Cefuroxime in Human Urine. *Anal. Chem.* **2018**, *90*, 13243–13248. [CrossRef]
32. Boisde, G.; Harmer, A. *Chemical and Biochemical Sensing With Optical Fibers and Waveguides*; Artech House: Boston, MA, USA, 1996.
33. Xiao, L.; Jin, W.; Demokan, M.S.; Ho, H.L.; Hoo, Y.L.; Zhao, C. Fabrication of selective injection microstructured optical fibers with a conventional fusion splicer. *Opt. Express* **2005**, *13*, 3412–3417. [CrossRef]
34. Ferraro, J.R.; Nakamoto, K.; Brown, C.W. *Introductory Raman Spectroscopy*; Academic Press: San Diego, CA, USA, 2003.
35. Eftekhari, F.; Irizar, J.; Hulbert, L.; Helmy, A.S. A comparative study of Raman enhancement in capillaries. *J. Appl. Phys.* **2011**, *109*, 113104. [CrossRef]

36. Weik, M.H. *Fibre Optics Standard Dictionary*; Chapman and Hall: New York, NY, USA, 1997.
37. Lan, G.-L.; Banerjee, P.K.; Mitra, S.S. Raman scattering in optical fibers. *J. Raman Spectrosc.* **1981**, *11*, 416–423. [CrossRef]
38. Carey, D.M.; Korenowski, G.M. Measurement of the Raman spectrum of liquid water. *J. Chem. Phys.* **1998**, *108*, 2669–2675. [CrossRef]
39. Jones, C.H.; Wesley, I.J. A preliminary study of the Fourier transform Raman spectra of polystyrenes. *Spectrochim. Acta A* **1991**, *47*, 1293–1298. [CrossRef]
40. Nielsen, L. Evaluation of measurements by the method of least squares. In *Algorithms for Approximation IV*; Levesley, J., Anderson, I.J., Mason, J.C., Eds.; University of Huddersfield: Huddersfield, UK, 2002; pp. 170–186.
41. Mätzler, C. MATLAB functions for Mie scattering and absorption, version 2. *IAP Res. Rep* **2002**, *8*, 1–24.
42. Rugeland, P.; Sterner, C.; Margulis, W. Visible light guidance in silica capillaries by antiresonant reflection. *Opt. Express* **2013**, *21*, 29217–29222. [CrossRef]
43. Frosch, T.; Yan, D.; Popp, J. Ultrasensitive Fiber Enhanced UV Resonance Raman Sensing of Drugs. *Anal. Chem.* **2013**, *85*, 6264–6271. [CrossRef]
44. Kerdoncuff, H.; Pollard, M.R.; Westergaard, P.G.; Lassen, M. Compact and versatile laser system for polarization-sensitive stimulated Raman spectroscopy. *Opt. Express* **2017**, *25*, 5618–5625. [CrossRef]

© 2020 by the authors. Licensee MDPI, Basel, Switzerland. This article is an open access article distributed under the terms and conditions of the Creative Commons Attribution (CC BY) license (http://creativecommons.org/licenses/by/4.0/).